

# Correlation between Small-Angle X-ray Scattering Spectra and Apparent Diffusion Coefficients in the Study of Structure and Interaction of Sodium Taurodeoxycholate Micelles

Sara Cozzolino,<sup>†</sup> Luciano Galantini,<sup>\*,†,‡</sup> Claudia Leggio,<sup>†,‡</sup> and Nicolae Viorel Pavel<sup>†,‡</sup>

Dipartimento di Chimica, Università di Roma "La Sapienza", P. le A. Moro 5, 00185 Roma, Italy, and INFM CRS-SOFT, c/o Università di Roma "La Sapienza", P. le A. Moro 5, 00185 Roma, Italy

Received: December 1, 2004; In Final Form: January 20, 2005

Small-Angle X-ray Scattering (SAXS) and Dynamic Light Scattering (DLS) measurements were carried out on aqueous micellar solutions of the ionic biological detergent sodium taurodeoxycholate (NaTDC). Apparent diffusion coefficients ( $D_{\text{app}}$ ) and SAXS spectra of NaTDC 0.1 M solutions at different ionic strengths (0.1–0.3 M NaCl) were reported. A comparative analysis of SAXS spectra and  $D_{\text{app}}$  data was performed to infer information on particle structure and interaction potential. Uniform particles with a spherical, an oblate, and a prolate symmetry were used to model the micelles in the data interpretation. A hard-core interaction shell of suitable thickness and a screened Coulomb potential of the electric double layer (EDL potential) were alternatively used to represent the long-range repulsive tail of the interaction potential. The Percus Yevick and the Rescaled Mean Spherical Approximation were applied. To compare the data of the two techniques, for each sample, a  $D_{\text{app}}$  was calculated from the SAXS best-fitting geometrical parameters and interparticle structure factor of the micelles. Hence, a fitting procedure involving both the scattering and  $D_{\text{app}}$  data was performed. The interpretation of SAXS spectra does not allow the discrimination between the oblate and the prolate symmetries of the aggregates. On the other hand, the comparison of calculated and experimental  $D_{\text{app}}$  values indicates that the prolate ellipsoid is better suited to represent the micelle shape. Moreover, the agreement between calculated and experimental  $D_{\text{app}}$  values is sensitively better at the lowest NaCl concentration when the EDL potential is used. A rodlike micellar growth and a progressive screening of the electrostatic interactions is testified by the trends of best-fitting parameters as a function of the added electrolyte.

## Introduction

In the characterization of colloids the measurements of translational diffusion coefficients are very often used to determine size and shape of colloidal particles.<sup>1–20</sup> The fundamental principle in the interpretation of these measurements is that the diffusion coefficient of colloidal particles in a solution may be calculated by treating the solute as a system of hydrodynamic particles immersed in a continuum solvent. In such cases, for infinitely diluted solutions, the diffusion coefficients of the solute particles are determined by the particle hydrodynamic radius that is related to their size and shape, and by the temperature and the viscosity of the solvent. It is well-known, however, that these diffusion coefficients depend on particle concentration. The interparticle interactions constitute the cause of such concentration dependence. In the measurements the interactions are generally regarded as a nuisance whose effect can be removed by extrapolation of data to zero concentration. Sometimes the concentration dependence of the data in the dilute region is analyzed to get information on the particle interaction potential.<sup>3–10</sup>

However, this kind of extrapolation cannot be reliably performed in the case of micellar systems where a growth of the micelles is often induced by increasing the surfactant

concentration. Therefore, an estimation of the particle interaction effect on the experimental data is needed to extract information on particle structure.

Dynamic light scattering (DLS) has been extensively used to estimate the diffusion coefficients of micelles.<sup>2–20</sup> However, in these measurements, the data were generally interpreted by assuming drastic hypotheses on the micelle behavior. In solutions of ionic micelles at low NaCl concentration it was supposed that no micelle growth is induced by increasing the surfactant concentration, thus justifying the extrapolation method in the data analysis.<sup>6–10</sup> On the other hand, an interaction potential constituted by just the excluded volume component was adopted to interpret the concentration dependence of the diffusion coefficients at high ionic strength to highlight the micellar growth effect.<sup>12</sup>

Static scattering techniques such as Small-Angle X-ray Scattering (SAXS) represent well-suited methods for investigating the structure of colloidal particles.<sup>21–28</sup> A small angle scattering experiment measures the intensity pattern as a function of the scattering vector of the coherently scattered radiation that is constructed by the arrangement of scattering centers in solution. Therefore, it is a function of the distribution of these centers within the particles and of the particle distribution within the solution. This means that particle structure and interparticle interactions determine the pattern of scattering spectra of colloidal solutions. However, as for the diffusivity data, the separation of these two effects cannot be achieved without some rigid assumption on particle structure and interaction potential.

\* Address correspondence to this author. Dipartimento di Chimica, Università di Roma "La Sapienza". Phone: (+39)-06-49913687. Fax: (+39)-06-490631. E-mail: l.galantini@caspur.it.

<sup>†</sup> Dipartimento di Chimica.

<sup>‡</sup> INFM CRS-SOFT.

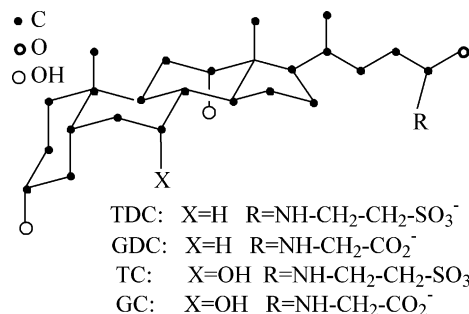


**Figure 1.** Formulas of some bile salt anions. The symbols TDC, GDC, TC, and GC refer to taurodeoxycholate, glycodeoxycholate, taurocholate, and glycocholate anions, respectively.

The number of these assumptions can be minimized if scattering and diffusivity measurements are integrated in a single interpretation. Recently some procedures based on the comparative analysis of SAXS and diffusivity measurements have been proposed to separate particle structure and particle interaction information on ionic micelle systems. They were tested on micellar solutions of some bile salts. In particular, solutions of cylindrical micelles of sodium glycodeoxycholate (NaGDC) at different added NaCl concentration were investigated by SAXS and DLS.<sup>22</sup>

A SAXS and DLS study was carried out in this paper on the micellar solution of sodium taurodeoxycholate (NaTDC) at 0.1–0.3 M NaCl, where the electrostatic repulsion dominates the interaction potential. The SAXS spectra were fitted by using the rescaled mean spherical approximation (RMSA)<sup>29</sup> to estimate the interparticle structure factor  $S(q)$ . Moreover, a model constituted by particles with a suitable hard interaction shell was also used to interpret SAXS spectra. The Percus–Yevick (PY)<sup>30</sup> approximation was applied in this case to estimate  $S(q)$ . With the same assumptions, apparent diffusion coefficients were calculated from the best-fitting SAXS parameters and compared with the experimental ones. The behavior of NaGDC and NaTDC micellar solutions is very similar. Both give rise to a remarkable micellar growth as a function of surfactant concentration and/or ionic strength.<sup>12,14,16,20,22</sup> As for more conventional amphiphiles this growth brings the formation of elongated aggregates.<sup>12,18,20,22–25</sup> However, spherical, oblate, and prolate symmetries of the micelles were assumed in the analysis in order to test the diagnostic ability of the comparative approach in the determination of the colloidal particle structure.

## Theoretical Background

**SAXS Data Treatment.** The contribution of a single particle to the total scattered intensity is generally expressed in terms of scattering form factor  $F(q)$  defined as

$$F(q) = \int \Delta\rho \exp(iq \cdot r) dV$$

where  $\Delta\rho$  is the difference between the particle and the solvent electron density and  $q = 4\pi \sin\theta/\lambda$  is the scattering vector. The integral is over the volume  $V$  of the particle. In the case of diluted solutions, particle interactions can be neglected and the form factor alone describes the scattered intensity. On the other hand, in a solution of interacting particles, correlation among the particles must be considered. For a monodisperse system of homogeneous and spherically symmetric particles the intensity can be factored into separate intra- and interparticle functions as

$$I(q) = N_p P(q) S(q) \quad (1)$$

where  $N_p$  is the particle number density,  $P(q)$  is the intraparticle structure factor that, for a homogeneous sphere with radius  $a$ , is given by

$$P(q) = |F(q)|^2 = \left[ 4\pi\Delta\rho \frac{\sin(qa) - qa \cos(qa)}{q^3} \right]^2 \quad (2)$$

and  $S(q)$  is the interparticle structure factor, which is related to the particle distribution within the solution and, as a function of the dimensionless distance  $x = r/2a$ , can be expressed as

$$S(q) = 1 + 24\phi \int_0^\infty x^2 [g(x) - 1] \frac{\sin(2aqx)}{2aqx} dx \quad (3)$$

where  $g(x)$  is the radial distribution function and  $\phi$  is the particle volume fraction. In the case of systems of nonspherically symmetric but monodispersed particles, the decoupling approximation can be assumed, and the scattered intensity expression can be generalized to<sup>22–27</sup>

$$I(q) = N_p P(q) \bar{S}(q) \quad (4)$$

where

$$P(q) = \langle |F(q)|^2 \rangle \quad (5)$$

$$\bar{S}(q) = 1 + \beta_o [S(q) - 1] \quad (6)$$

$$\beta_o = \frac{\langle |F(q)|^2 \rangle}{\langle |F(q)|^2 \rangle} \quad (7)$$

with the angular brackets representing the average over all the particle orientations.

For ellipsoids with semimajor axis  $a_e$  and semiminor axis  $b_e$  the following form factor orientational averages must be used in eqs 5 and 7<sup>26</sup>

$$\langle |F(q)|^2 \rangle = \int_0^{\pi/2} |F(q, a_e, b_e, \beta)|^2 \sin\beta d\beta \quad (8)$$

$$\langle |F(q)|^2 \rangle = \left| \int_0^{\pi/2} F(q, a_e, b_e, \beta) \sin\beta d\beta \right|^2 \quad (9)$$

where, for homogeneous prolate ellipsoids

$$F(q, a_e, b_e, \beta) = 4\pi a_e^2 b_e^2 \Delta\rho \frac{J_1\{q[(a_e \cos\beta)^2 + (b_e \sin\beta)^2]^{1/2}\}}{q[(a_e \cos\beta)^2 + (b_e \sin\beta)^2]^{1/2}} \quad (10)$$

and for oblate ellipsoids

$$F(q, a_e, b_e, \beta) = 4\pi a_e^2 b_e^2 \Delta\rho \frac{J_1\{q[(a_e \sin\beta)^2 + (b_e \cos\beta)^2]^{1/2}\}}{q[(a_e \sin\beta)^2 + (b_e \cos\beta)^2]^{1/2}} \quad (11)$$

where  $J_1$  represents a first-order Bessel function and  $\beta$  is the orientation angle.

**DLS Data Treatment.** In general, a dynamic particle solution gives rise to a time-varying scattered intensity because of the particle Brownian motion. In a DLS experiment the temporal fluctuations of the scattered intensity are analyzed by estimating the normalized intensity–intensity time autocorrelation function  $g_2(q, \tau)$ .

For a Gaussian distribution of the intensity profile,  $g_2(q, \tau)$  is related to the normalized field autocorrelation

function  $g_1(q, \tau)$  as<sup>31,32</sup>

$$g_2(q, \tau) = 1 + B|g_1(q, \tau)|^2$$

In the most general cases  $g_1(q, \tau)$  is analyzed through the cumulant expansion and the apparent diffusion coefficient  $D_{app}$  is obtained from the first cumulant by the relation

$$D_{app} = -\frac{1}{q^2} \left. \frac{d \ln g_1(q, \tau)}{d\tau} \right|_{\tau=0}$$

Because of particle interactions it is expected that  $D_{app}$  depends on the scattering vector. A general expression for this diffusion coefficient is given by<sup>9,33,34</sup>

$$D_{app} = \frac{D_o[1 + H(q)]}{S(q)} \quad (12)$$

where  $H(q)$  is the hydrodynamic function that accounts for the flow related interactions, and  $D_o$  represents the diffusion coefficient at infinite dilution given by

$$D_o = \frac{kT}{6\pi\eta a_h} \quad (13)$$

with  $k$ ,  $T$ ,  $a_h$ , and  $\eta$  representing the Boltzmann constant, the absolute temperature, the hydrodynamic radius of the diffusing particles, and the medium viscosity, respectively. In the hydrodynamic limit, where we performed our measurements, the characteristic probing length of the scattering experiment ( $2\pi/q$ ) is much larger than the most probable particle distance. In this case the limit  $q \rightarrow 0$  of eq 12 can be considered and the apparent diffusion coefficient can be written as

$$D_{app} = D_o \frac{1 - \lambda_f \phi}{S(0)} \quad (14)$$

The term  $\lambda_f$  depends on particle distribution and can be expressed in an integral form as a function of  $g(x)$  as

$$\lambda_f = \lambda_{fo} + \int_1^\infty F(x)[1 - g(x)] dx \quad (15)$$

where, according to the Felderhof treatment,<sup>35</sup> we have  $\lambda_{fo} = 6.44$  and

$$F(x) = 12x - \frac{15}{8x^2} + \frac{27}{64x^4} + \frac{75}{64x^5} \quad (16)$$

A fundamental result of the theory so far reported is that the effect of particle interactions on scattering and diffusivity measurements can be quantified if the  $g(x)$  is known. This function can be calculated from liquid state theory by solving the Ornstein–Zernike (OZ) equation for the total correlation function  $h(x) = g(x) - 1$ .<sup>36</sup> Actually, to solve the OZ equation additional closure relations are required. The closure conditions are in general approximations and are commonly chosen on the basis of the particle interaction potential features. The RMSA and the PY approximations are used in this paper. In a system of spherical particles, if a suitable guess of the interaction potential is available, these relations provide procedures for determining the  $S(q)$  and  $g(x)$  functions, which are related by the Fourier transform of eq 3, and then the  $\lambda_f$  value by means of eqs 15 and 16. For slightly anisotropic particles, these methods can still be applied to determine  $g(x)$  and  $S(q)$  by assuming the particles being represented by equivalent spheres.

In the case of elongated particles, the radius of the equivalent sphere is determined by equating the second virial coefficient of the ellipsoidal particle system to the second virial coefficient of a hard sphere solution. Moreover, in the case of a not pronounced anisotropy of the particle shape, the hydrodynamic interaction can be treated as for spherical particles, thus preserving the form of eqs 14, 15, and 16. This means that these interactions are represented as those which take place between spheres with the volume of the anisotropic particles.

In this frame the RMSA and the PY approximation can be used to fit the SAXS spectra, thus providing the geometrical parameters of the micelles and the  $S(q)$  function. At the same time these approximations can be applied to interpret the  $D_{app}$  data. On the basis of these considerations a study is carried out in this paper where a comparison of SAXS and  $D_{app}$  data is performed and, finally, an overall fit of the two sets of data is attempted.

A crucial parameter in these data correlation is represented by the micelle volume fraction  $\phi$  that is fundamental in the description of the micelle distribution in a sample. Starting from the critical micelle concentration (cmc) and assuming a specific micellar volume per monomer  $v$ , we estimated this fraction as  $\phi = (c - \text{cmc})N_A v$ ,  $c$  and  $N_A$  being the total surfactant molar concentration and the Avogadro constant, respectively. A reasonable  $v$  value could be obtained from the NaTDC molar volume  $V$  as  $v = V/N_A = 608 \text{ \AA}^3$ .<sup>37</sup> Actually this value is underestimated since it does not consider the hydration water molecule contribution to the micelle volume. From the comparison of apparent and self-diffusion coefficients  $v = 734 \text{ \AA}^3$  was estimated for micellar aggregates of sodium taurocholate (NaTC).<sup>13</sup> Moreover, in view of the similarity of NaTDC and NaTC molecules this  $v$  value was successfully used to interpret diffusivity data of NaTDC micelles.<sup>20</sup> This value is considered also in this paper to interpret both the  $D_{app}$  and the SAXS data. It is important to note that, since the same  $v$  is assumed to correlate the two techniques, it is implicit that the same particle geometry is supposed to describe the scattering and the hydrodynamic properties of the micelles.

As a function of  $v$ , whenever the scattered intensity  $I(q)$  was estimated in this work, an aggregation number  $n$  and a number density of micelles  $N_p$  were calculated as  $n = v_m/v$  and  $N_p = N_A(c - \text{cmc})/n$ , where  $v_m$  is the micellar volume, which is strictly related to the micellar structure. No hypothesis on  $\Delta\rho$  in eqs 2, 10, and 11 was made a priori. This means that in the comparison with the experimental scattering curves the  $\Delta\rho$  value in the calculated  $I(q)$  was always assumed as the scale factor, which gives the best agreement with the measured intensities.

## Experimental Section

**Materials.** NaTDC (Sigma) and NaCl (Merck, suprapur) were used. The NaTDC was twice crystallized from water and acetone before sample preparation. The first aggregation cmc values of ref 38 were considered in the calculation. The highest cmc value reported in this reference, corresponding to the aqueous solution of NaTDC without added NaCl, is 2.9 mM, which is much lower than the NaTDC concentration studied in this work (0.1 M).

**DLS Measurements.** A Brookhaven instrument constituted by a BI-2030AT digital correlator with 136 channels and a BI-200SM goniometer was used. The light source was a Uniphase solid-state laser system model 4601 operating at 532 nm. Dust was eliminated by means of a Brookhaven ultrafiltration unit (BIUU1) for flow-through cells, the volume of the flow cell being about 1.0 mL. Nucleopore filters with a pore size of 0.1  $\mu\text{m}$  were used. The samples were placed in the cell for at least

30 min prior the measurement to allow for thermal equilibration. Their temperature was kept constant within 0.5 °C by a circulating water bath. The time-dependent light scattering correlation function was analyzed only at the 90° scattering angle. Apparent diffusion coefficients did not depend on the exchanged wave vector in the range 30–150° in our experimental conditions.

**SAXS Measurements.** The measurements were carried out in a quartz capillary of 1 mm by using a Kratky compact system equipped with a NaI scintillation counter in a temperature-controlled room at  $25 \pm 1$  °C. Ni-filtered Cu K $\alpha$  radiation ( $\lambda = 1.5418$  Å) was used. Scattering curves were recorded within the range  $0.012 \leq q \leq 0.5$  Å<sup>-1</sup>. The moving slit method was employed to measure the intensity of the primary beam and the scattering intensities were put on an absolute scale.<sup>39</sup> The absolute scale is expressed in electrons<sup>2</sup> Å<sup>-3</sup> and electrons<sup>2</sup> Å<sup>-3</sup> cm length of the primary beam for desmeared and smeared intensities, respectively. In the minimization procedures, the calculated intensities have been smeared by the normalized weighting functions for slit length and slit width effects<sup>40</sup> and the best agreement with the experimental data was obtained by minimizing the function

$$R = \frac{1}{N} \sum_{i=1}^N \frac{(I_o(q) - I_c(q))^2}{\sigma_i^2}$$

where  $I_o(q)$  and  $I_c(q)$  are the smeared observed and calculated intensities,  $\sigma_i^2$  is the  $I_o(q)$  variance, and  $N$  is the number of experimental points.

## Results and Discussion

**SAXS Data Interpretation.** SAXS and DLS measurements were carried out on NaTDC 0.1 M aqueous solutions at different NaCl concentrations (Figures 2 and 5). A decrease of  $D_{app}$  by increasing the ionic strength is observed. This trend was related to a micellar growth and a progressive screening of the electrostatic repulsions in a previous paper.<sup>20</sup> It is obvious from the theoretical treatment section that both the apparent diffusion coefficients and the SAXS spectra are affected by particle direct interactions that determine the radial distribution function pattern. It is reported in the literature that in many cases the micelle–micelle direct interaction can be well approximated as a sum of a hard body repulsion or excluded volume component plus a long-range interaction potential tail. On the basis of the DLVO theory of colloidal stability,<sup>41</sup> for ionic micelles, this tail can be considered as a combination of two independent components: (i) an electric double layer repulsion between the two charged micelles with their ionic atmospheres and (ii) a van der Waals attraction. At low electrolyte concentration the electrostatic repulsion term prevails on the attractive one. However, the electrostatic component is screened by increasing the electrolyte concentration and when a sufficient amount of electrolyte is added the intermicellar attraction prevails. Therefore we can imagine that the interaction potential tail presents a character that is essentially repulsive or attractive at low or high ionic strength, respectively. This phenomenon was highlighted in a previous paper by comparing  $D_{app}$  data and Pulse gradient spin–echo <sup>1</sup>H NMR self-diffusion coefficients on NaTDC D<sub>2</sub>O solutions at different NaCl concentrations.<sup>20</sup> In the same paper we demonstrated that the electrostatic repulsion dominates the potential tail up to about 0.3 M NaCl concentration. Of course, the variation of the interaction potential affects the electrolyte concentration dependence of SAXS and

**TABLE 1: Best Fitting Parameters of SAXS Spectra Assuming a Spherical Shape of the NaTDC Micelles on the Basis of the HC and the EDL Interaction Models, as a Function of NaCl Concentration<sup>a</sup>**

NaCl (mM)	HC model		EDL model		
	$a$ (Å)	$t$ (Å)	$a$ (Å)	$\alpha$	$\kappa^{-1}$ (Å)
100	21.8	7.65	21.8	0.300	8.88
150	22.6	7.10	22.4	0.310	7.45
200	23.2	1.85	23.0	0.131	6.68
250	23.4	0.0	23.4	0.0	6.07
300	24.8	0.0	24.8	0.0	5.54

<sup>a</sup> Esd's are within 0.1 Å ( $a$ ), 0.05 Å ( $t$ ), 0.002 ( $\alpha$ ), and 0.05 Å ( $\kappa^{-1}$ ).

DLS data of Figures 2 and 5. However, a marked micellar growth is also expected to influence these data.

Despite the elongated shape that is in general proposed for the NaTDC micelles, as a first approach we performed the data analysis by assuming a spherical symmetry of the micelles. In this way, the micellar aggregates were supposed to have a radius  $a$  and a volume  $v_m = 4\pi a^3/3$ . On the basis of the DLVO theory of colloid stability, the electrostatic repulsive component  $V(x)$  of the interaction potential between two spherical ionic micelles can be obtained from the solution of the Poisson–Boltzmann equation for the charged double layer. At low ionic strength the analytical form of this potential is given by

$$V(x) = \frac{n^2 \alpha^2 e^2}{8\pi \epsilon_0 \epsilon_a (1 + \kappa a)^2} \frac{\exp[-2\kappa a(x - 1)]}{x} \quad (17)$$

where  $\epsilon$  is the dielectric constant of the medium,  $\epsilon_0$  is the permittivity of the free space,  $\alpha$  is the ionization degree,  $e$  is the electronic charge, and  $\kappa$  is the Debye–Hückel inverse screening length defined as

$$\kappa = \left( \frac{N_A e^2 I \times 10^3}{k T \epsilon \epsilon_0} \right)^{1/2}$$

where  $I = 2(\text{cmc} + c_{\text{NaCl}}) + \alpha(c - \text{cmc})$ ,  $c_{\text{NaCl}}$  being the NaCl molarity.

By neglecting the van der Waals attractive contribution, generally the electric double layer (EDL) potential of eq 17 is used to represent the tail of the interaction potential in micellar systems at low ionic strength (EDL interaction model). The main reason of this choice is that the  $S(q)$  can be easily estimated by using the RMSA.<sup>29</sup> This method was used to interpret the NaTDC spectra at NaCl concentration  $\leq 0.3$  M. During the minimization procedure  $a$  and  $\alpha$  were varied. The best-fitting curves are reported in Figure 2 and the corresponding parameters  $a$ ,  $\alpha$ , and  $\kappa^{-1}$  are listed in Table 1.

It is important to note that, according to the DLVO theory at high electrolyte concentration, where  $\kappa^{-1}$  is much smaller than the micellar sizes, eq 17 cannot be used to describe the electric double layer potential. Because of this problem the EDL model is generally applied only at low ionic strength where the electrostatic component still can be represented by eq 17. In a small-angle neutron-scattering study reported in the literature, the fit at higher ionic strength was performed by using a more general model than the EDL one.<sup>25</sup> In this model (HC model), a rigid interaction shell was assumed to mimic the effect of the essentially repulsive tail characterizing the intermicellar interaction potential. In our case both the HC and the EDL interaction models were applied to fit the SAXS spectra at all the studied NaCl concentrations in order to verify their applicability in the description of the particle interaction. To represent the inter-



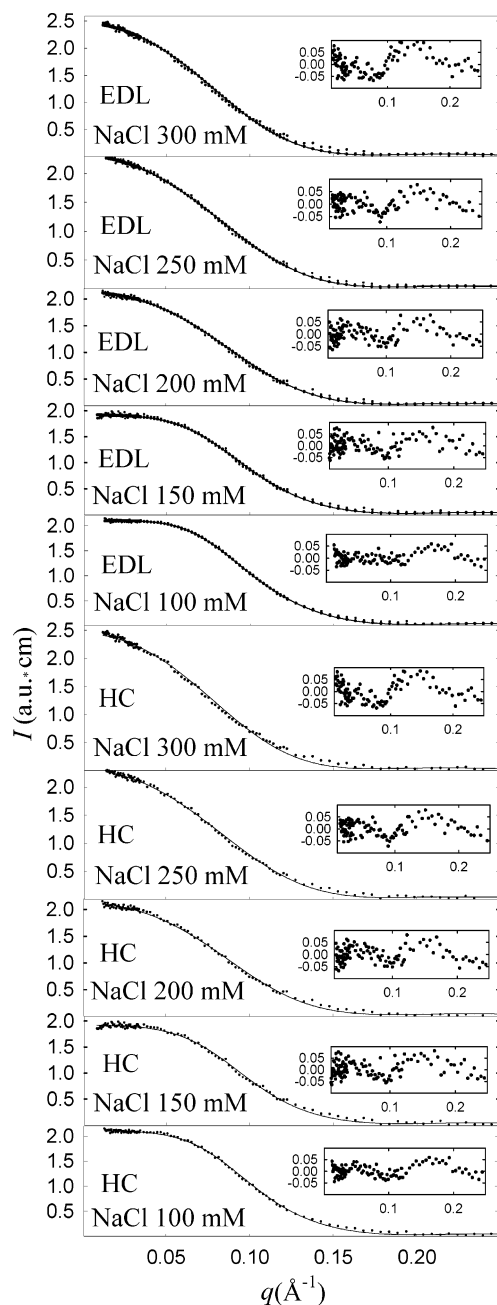


**Figure 2.** SAXS spectra of 0.1 M NaTDC micellar solutions at different NaCl concentrations and at 25 °C (dots). The solid lines are the theoretical fits on the basis of the HC (HC panels) or the EDL (EDL panels) interaction models by assuming a spherical shape of the micelles. The residuals are reported in the insets.

particle repulsion in the HC model, the micellar aggregates were supposed to give a hard interaction at a radius  $a + t$ ,  $a$  and  $t$  being the micellar radius and the interaction shell thickness, respectively.<sup>13,20,22,42,43</sup> Both these parameters were varied in the minimization procedure and, for each couple of values, the  $S(q)$  function was estimated by applying the PY closure approximation to the system of hard spheres with radius  $a + t$ .<sup>44,45</sup> The best-fitting curves are reported in Figure 2 and the corresponding  $a$  and  $t$  values are reported in Table 1.

In a second step the anisotropic shape of the micelles was taken into account. Therefore, interpretation models of ellipsoidal particles were used to represent the micelle. Both homogeneous oblate and prolate ellipsoids were tested and the decoupling approximation was assumed to fit the SAXS spectra eqs 4–11. Spherical particles with the same virial coefficient

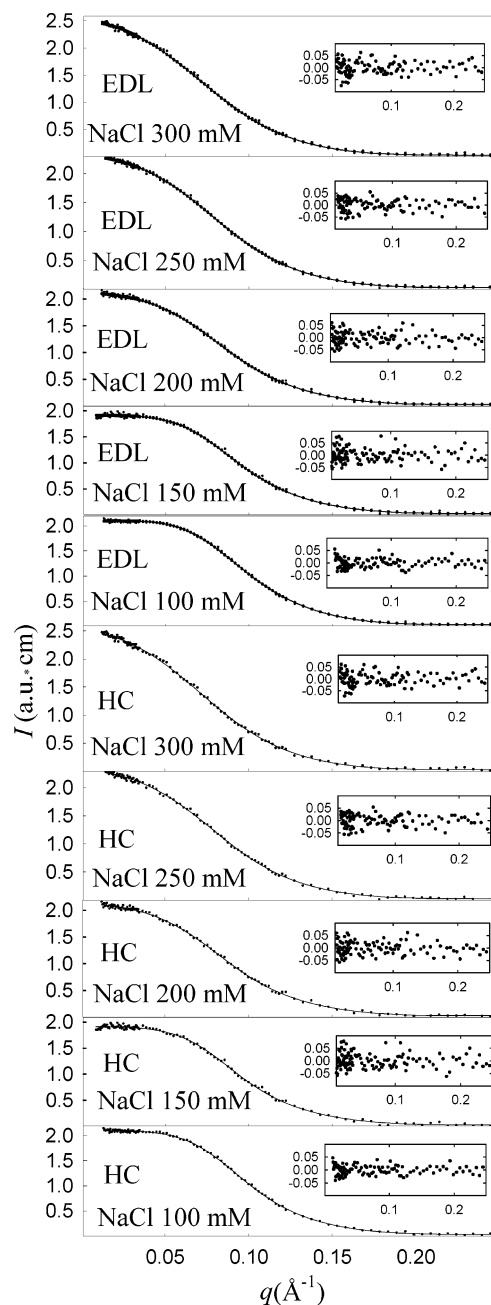


**Figure 3.** SAXS spectra of 0.1 M NaTDC micellar solutions at different NaCl concentrations and at 25 °C (dots). The solid lines are the theoretical fits on the basis of the HC (HC panels) or the EDL (EDL panels) interaction models and of a prolate ellipsoidal shape of the micelles. The residuals are reported in the insets.

of the ellipsoids were assumed to determine the  $S(q)$  function under the hypothesis of the EDL interaction model, on the basis of RMSA. A homogeneous thickness of the interaction shell was considered in the HC interaction model. This means that for ellipsoidal particles with semi axes  $a_e$  and  $b_e$  an interaction ellipsoid of semi axis  $a_e + t$  and  $b_e + t$ ,  $t$  being the interaction shell thickness, was assumed. The  $S(q)$  was calculated by applying the PY approximation on hard spheres with the same virial coefficient of the interaction ellipsoids. The best-fitting curves for both the HC and the EDL interaction models are reported in Figures 3 and 4 for prolate and oblate symmetries of the particles. As shown by the residual patterns, the SAXS fits markedly improve with respect to the spherical case (Figure 2). The best-fitting SAXS parameters obtained with this

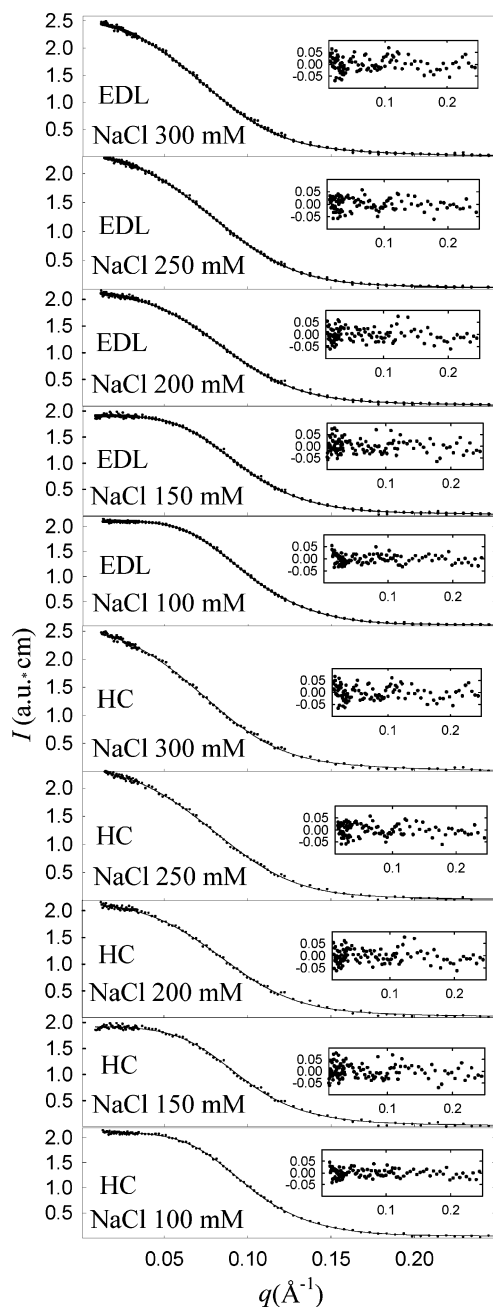


**Figure 4.** SAXS spectra of 0.1 M NaTDC micellar solutions at different NaCl concentrations and at 25 °C (dots). The solid lines are the theoretical fits on the basis of the HC (HC panels) or the EDL (EDL panels) interaction models and of an oblate ellipsoidal shape of the micelles. The residuals are reported in the insets.

treatment are reported in Tables 2 and 3 for the prolate and the oblate cases, respectively.

As pointed out from the comparison of the best-fitting curves of Figure 2 and those of Figures 3 and 4 the ellipsoids give better fits of the experimental spectra. This means that the sphere is unsuitable to describe the NaTDC micelles. However, on the basis of the fits of Figures 3 and 4 nothing can be said on the ellipsoidal symmetry that better represents the NaTDC micelles since both the prolate and the oblate geometries give a good agreement of experimental and calculated intensities. In view of these results we carried out the comparative analysis of  $D_{app}$  and SAXS spectra by using all three geometrical models. The main reason for this analysis is to show what happens to the agreement of the compared data when suitable or unsuitable micellar shapes are assumed. In this way we can verify if the

**TABLE 2: Best Fitting Parameters of SAXS Spectra Assuming a Prolate Ellipsoidal Shape of the NaTDC Micelles on the Basis of the HC and the EDL Interaction Models, as a Function of NaCl Concentration<sup>a</sup>**

NaCl (mM)	HC model			EDL model			
	$a_e$ (Å)	$b_e$ (Å)	$t$ (Å)	$a_e$ (Å)	$b_e$ (Å)	$\alpha$	$\kappa^{-1}$ (Å)
100	31.4	18.5	8.05	30.0	18.7	0.317	8.85
150	35.6	18.4	7.90	34.2	18.6	0.380	7.37
200	41.4	18.5	4.55	39.8	18.6	0.230	6.60
250	41.2	18.9	2.60	39.8	19.0	0.170	5.97
300	45.0	19.3	0.85	43.4	19.4	0.060	5.52

<sup>a</sup> Esd's are within 0.1 Å ( $a_e$  and  $b_e$ ), 0.05 Å ( $t$ ), 0.002 ( $\alpha$ ), and 0.05 Å ( $\kappa^{-1}$ ).

**TABLE 3: Best Fitting Parameters of SAXS Spectra Assuming an Oblate Ellipsoidal Shape of the NaTDC Micelles on the Basis of the HC and the EDL Interaction Models, as a Function of NaCl Concentration<sup>a</sup>**

NaCl (mM)	HC model			EDL model			
	$a_e$ (Å)	$b_e$ (Å)	$t$ (Å)	$a_e$ (Å)	$b_e$ (Å)	$\alpha$	$\kappa^{-1}$ (Å)
100	25.9	15.7	8.05	25.4	16.1	0.315	8.85
150	27.5	15.3	7.45	27.1	15.6	0.360	7.40
200	29.0	15.3	3.30	28.6	15.5	0.185	6.63
250	28.9	15.9	0.92	28.8	15.9	0.100	6.01
300	31.6	15.2	0.05	31.6	15.4	0.020	5.54

<sup>a</sup> Esd's are within 0.1 Å ( $a_e$  and  $b_e$ ), 0.05 Å ( $t$ ), 0.002 ( $\alpha$ ), and 0.05 Å ( $\kappa^{-1}$ ).

SAXS and DLS data comparison allows the determination of the best suited geometry to represent the micelles, thus providing a method to discriminate between the oblate and the prolate shapes.

An inspection of Tables 1–3 shows that similar geometrical parameters of the micelles are obtained by using the HC or the EDL interaction model. The reported  $t$  values indicate that the interaction potential, which is strongly repulsive at low NaCl concentration, progressively loses its repulsive character by increasing the electrolyte molarity. The same effect is highlighted by a decrease of  $\alpha$  and  $\kappa^{-1}$ . However, the behavior of  $\alpha$  is very probably unrealistic. In fact, published results on bile salt and more conventional surfactant solutions demonstrate that, if the complete DLVO interaction potential is considered, namely both the attractive and the EDL repulsive components of the potential tail are taken into account, the effect of the added electrolyte can be ascribed simply to a screening of the double layer repulsion.<sup>10,42</sup> This effect is represented by a lowering of  $\kappa^{-1}$  because of the ionic strength increase without invoking any variation of the  $\alpha$  value. Since the attractive component is neglected in the EDL model the simple decrease of  $\kappa^{-1}$  is no more sufficient to represent the repulsion screening. This means that a significant lowering of  $\alpha$  is needed to allow the simple EDL interaction potential to account for the attractive contribution increase.

In Table 1 the  $t$  and  $\alpha$  values vanish at NaCl concentration  $\geq 250$  mM. This means that, on the basis of the SAXS spectra, when the spherical shape of the micelles is assumed, the interaction potential tail is surely not repulsive in these conditions. Nothing more can be said on the features of this tail. However, we can suspect that at these ionic strengths the repulsive character that we considered for the interaction potential could be a bad assumption for fitting the SAXS spectra under the hypothesis of the spherical micelles and probably the choice of an attractive tail could give rise to better fits. Obviously, the best-fitting parameters at NaCl concentration  $\geq 250$  mM in Table 1 are conditioned by the forced assumption of a repulsive character of the tail. Therefore, these parameters

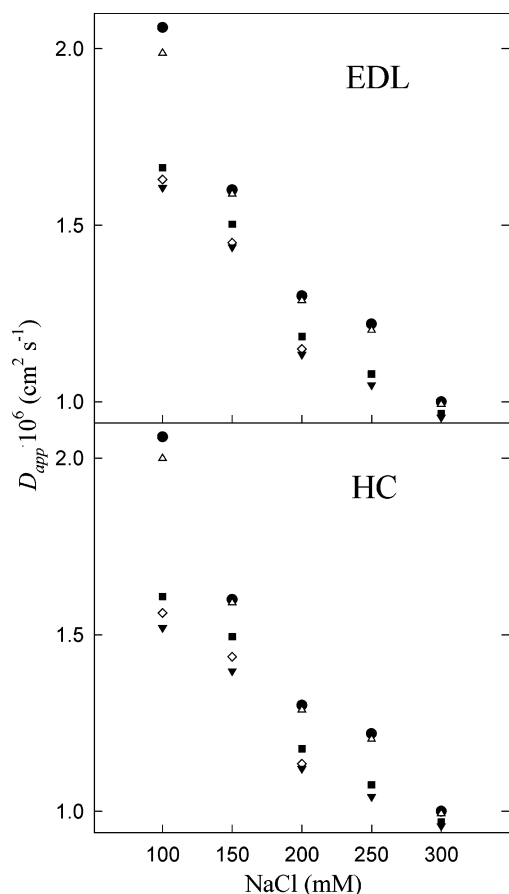


**Figure 5.** Experimental  $D_{app}$  (full circles) together with the  $D_{appS}$  values calculated for the SAXS best-fitting parameters of Tables 1–3 obtained on the basis of the HC (lower panel) and the EDL (upper panel) interaction models assuming a spherical (open diamonds), an oblate (down pointing solid triangles), or a prolate (solid squares) symmetry of the micelles. The  $D_{appSD}$  values (up pointing open triangles) estimated by minimizing the  $R_D$  function of eq 21 for the ellipsoidal model are also reported. The esd's are within 0.5%.

could be affected by an unsuitable choice not only of the micellar shape but also of the potential tail. Hence, they were discarded in the comparison with the  $D_{app}$  values.

**SAXS and DLS Data Correlation.** As described in the theoretical background section, the  $S(0)$  and the  $\lambda_f$  values must be known to quantify the effect of particle interactions on  $D_{app}$  (eq 14). As a first approach the SAXS best-fitting  $S(q)$  function can be used to calculate these parameters. This function at  $q = 0$  provides the  $S(0)$  value of eq 14. Moreover as shown in eq 3 the Fourier transform of  $S(q) - 1$  allows the calculation of the radial distribution function as

$$g(x) = 1 + \frac{4a^2}{12\pi\phi x} \int_0^\infty [S(q) - 1] q \sin(2qax) dq \quad (18)$$

and consequently the determination of  $\lambda_f$  by means of eqs 15 and 16.

Equations proposed by Perrin<sup>47</sup> are reported in the literature to calculate equivalent hydrodynamic radii ( $a_{heq}$ ) of ellipsoidal particles. In particular, for our ellipsoids, we have<sup>46–48</sup>

$$a_{heq} = \frac{a_e \gamma}{\ln \left[ \frac{a_e(1 + \gamma)}{b_e} \right]} \quad (19)$$

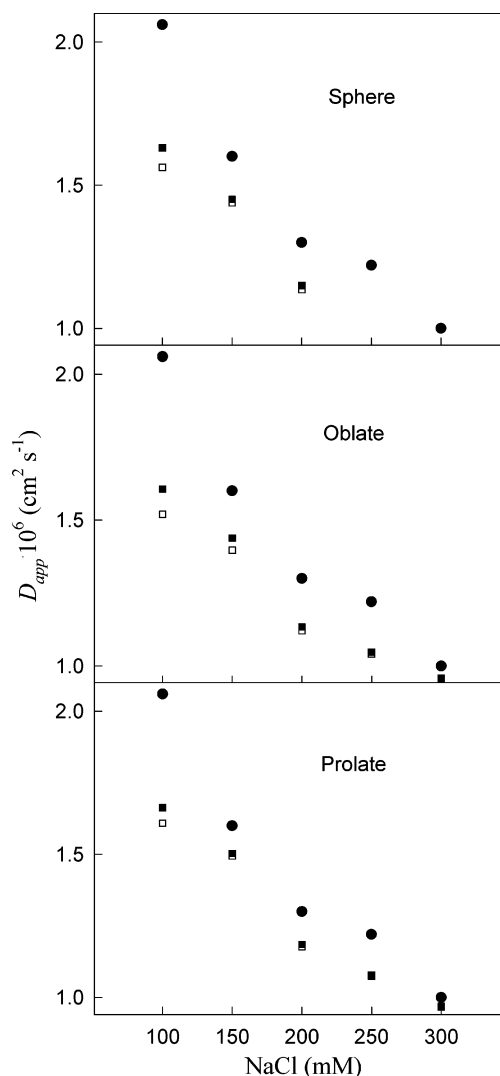


**Figure 6.** Experimental  $D_{app}$  (solid circles) together with the  $D_{appS}$  values calculated for the SAXS best-fitting parameters of Tables 1–3 obtained on the basis of the HC (open square) and the EDL (solid square) interaction models assuming a spherical, an oblate, or a prolate shape of the micelles. The esd's are within 0.5%.

where  $\gamma = [1 - (b_e^2/a_e^2)]^{1/2}$  in the case of prolates and

$$a_{heq} = \frac{b_e \gamma'}{\tan^{-1} \gamma'} \quad (20)$$

where  $\gamma' = [(a_e^2/b_e^2) - 1]^{1/2}$  in the case of oblates. From the SAXS best-fitting  $a_e$  and  $b_e$  values obtained assuming the ellipsoidal geometry of the micelles (Tables 2 and 3) equivalent hydrodynamic radii can be calculated by means of eqs 19 and 20. Therefore a  $D_o$  value ( $D_{oe}$ ) can be estimated by putting these  $a_{heq}$  values in eq 13. The same value can be obtained in the case of the spherical model by substituting in this equation the SAXS best-fitting  $a$  values of Table 1.

In this framework starting from the SAXS best-fitting geometrical parameters and  $S(q)$  function obtained from both the EDL and the HC interaction models,  $S(0)$ ,  $\lambda_f$ , and  $D_{oe}$  were estimated for each sample. Hence, assuming the  $\phi$  value as reported in the theoretical background section a SAXS best-fitting  $D_{app}$  ( $D_{appS}$ ) was obtained by using eq 14. The resulting data are compared on the basis of the geometrical or the interaction model in Figures 5 and 6, respectively.

As shown in Figure 5, the poorest agreement between the  $D_{appS}$  and experimental  $D_{app}$  values is obtained when the oblate

**TABLE 4: Best Fitting Parameters of SAXS and  $D_{app}$  Data Obtained by Minimizing  $R_D$  of Eq 21, Assuming a Prolate Ellipsoidal Shape of the NaTDC Micelles on the Basis of the HC and the EDL Interaction Models, as a Function of NaCl Concentration<sup>a</sup>**

NaCl (mM)	HC model				EDL model				
	$a_e$ (Å)	$b_e$ (Å)	$t$ (Å)	$a_{heq}$ (Å)	$a_e$ (Å)	$b_e$ (Å)	$\alpha$	$\kappa^{-1}$ (Å)	$a_{heq}$ (Å)
100	36.6	17.6	11.1	23.6	33.6	18.1	0.540	8.47	23.0
150	38.4	18.0	9.00	24.4	36.8	18.2	0.470	7.28	24.1
200	47.6	18.0	7.00	27.1	46.2	18.1	0.380	6.49	26.7
250	50.4	18.4	6.65	28.2	49.4	18.4	0.410	5.84	27.5
300	52.4	18.8	2.95	29.0	51.2	18.8	0.195	5.46	28.7

<sup>a</sup> Esd's are within 0.1 Å ( $a_e$ ,  $b_e$ , and  $a_{heq}$ ), 0.05 Å ( $t$ ), 0.002 ( $\alpha$ ), and 0.05 Å ( $\kappa^{-1}$ ).

shape is assumed for the micelles and slightly improves passing to the spherical case. The best agreement is obtained when the prolate micellar shape is considered, thus indicating that this is the best shape to describe the NaTDC micelles. This result confirms the information reported in the literature, which suggests that elongated aggregates are given by this surfactant.<sup>12,20</sup>

On the other hand, within the same geometrical model very similar  $D_{app}$  values are generally observed with the two interaction models (Figure 6). However, at the lowest NaCl concentration, a sensitively better agreement between  $D_{app}$  and  $D_{appS}$  values is observed when the EDL intermicellar potential is considered, thus indicating that the choice of the form of the potential tail can be crucial in the interpretation of scattering and diffusivity data and that the EDL form is clearly better suited than the HC one.

It must be stressed that, in this correlation of SAXS and DLS data, we treated the solutions in the frame of a single particle model. This means that we assumed the free monomers, the micelle counterions, and the NaCl ions as point-like particles with an instantaneous diffusion constant, namely that all the small ions are supposed to be involved only in the Debye screening parameter. Of course this is an approximation that could affect our results. However, it has been demonstrated that the errors induced by this assumption are relevant only at very low ionic strength and that they should be negligible at our electrolyte concentrations.<sup>49,50</sup>

The parameters defining the structure and the interaction potential of the micelles so far reported were obtained by fitting only the SAXS spectra. Actually, since the same interpretation model can be used to interpret SAXS and DLS measurements, an overall fit of both the SAXS and DLS data can be performed. This fit represents the best way to interpret the two experimental data, because it uses the largest number of available experimental points. In other words since the same number of fitting parameters is used, this fit is better conditioned than the one based on the SAXS spectra alone. In this frame, a new fitting procedure was executed involving both experimental data. In view of the results obtained in the previous comparative analysis, this new fitting procedure was applied only in the case of the best-suited model of prolate ellipsoidal micelles. The minimization was performed by varying systematically  $a_e$  and  $b_e$  together with  $t$  or  $\alpha$  in case of the HC or the EDL model, respectively. For each data set ( $a_e$ ,  $b_e$ , and  $t$  or  $a_e$ ,  $b_e$ , and  $\alpha$ ) the  $D_{appS}$  value was calculated as previously described for the best-fitting SAXS parameters of Table 2. Moreover, as in the fitting of the SAXS spectra, a calculated scattering intensity  $I_c(q)$  was estimated on the basis of the chosen interaction model. Hence, of all the examined data sets, the one that gives the best agreement with

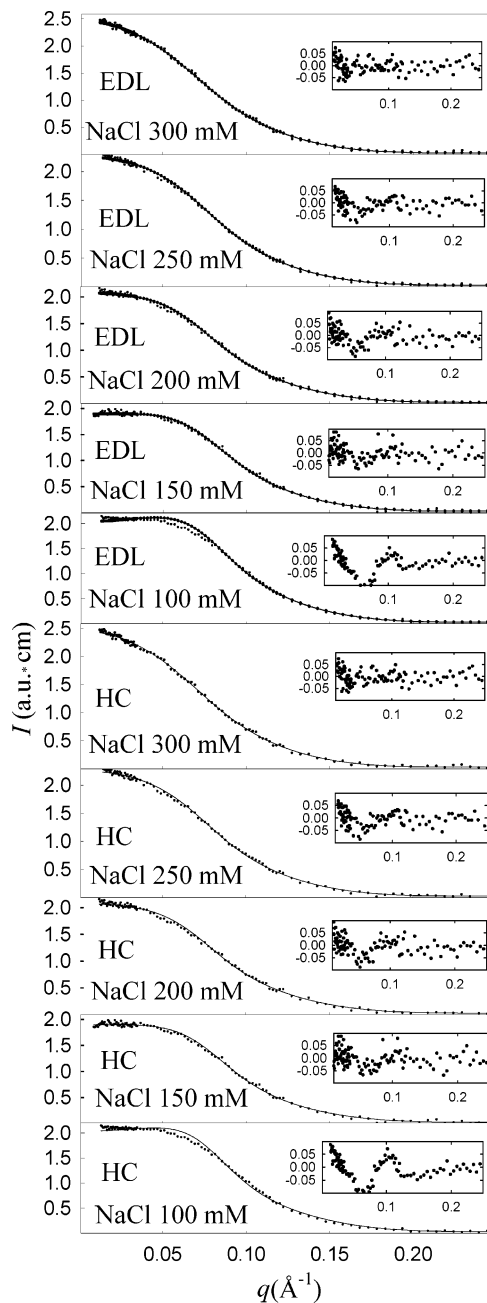


**Figure 7.** SAXS spectra of 0.1 M NaTDC micellar solutions at different NaCl concentrations and at 25 °C (dots). The solid lines are the theoretical fits on the basis of the HC (HC panels) or the EDL (EDL panels) interaction models and of a prolate ellipsoidal shape of the micelles obtained by minimizing the  $R_D$  function of eq 21. The residuals are reported in the insets.

both SAXS and  $D_{app}$  data was selected by imposing the minimum value of the function

$$R_D = \frac{1}{N+1} \left[ \frac{(D_{app} - D_{appS})^2}{\sigma_D^2} + \sum_{i=1}^N \frac{(I_o(q) - I_c(q))^2}{\sigma_i^2} \right] \quad (21)$$

where  $\sigma_D$  is the estimated standard deviation of the experimental  $D_{app}$ . The best-fitting parameters obtained with this procedure are reported in Table 4. In the same table the equivalent hydrodynamic radii ( $a_{heq}$ ) calculated from the best-fitting  $a_e$  and  $b_e$  values by means of eq 19 are also reported.

The best-fitting intensity curves are superimposed on the experimental spectra in Figure 7. The corresponding  $S(q)$



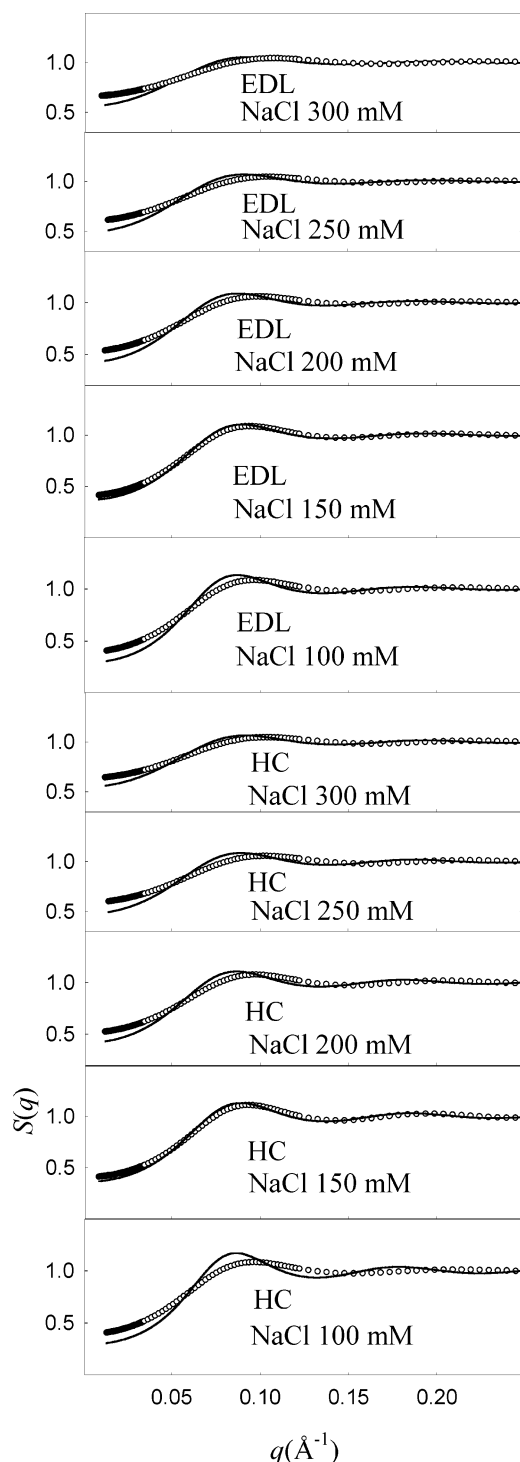


**Figure 8.** The extracted  $S(q)$  of the best-fitting  $I(q)$  curves of Figure 4 (open circles) and of Figure 8 (solid lines).

functions are reported in Figure 8 together with the patterns extracted from the best-fitting curves of Figure 3. The best-fitting  $D_{\text{appSD}}$  values ( $D_{\text{appSD}}$ ) are reported in Figure 5.

The comparison of the  $D_{\text{appSD}}$  values with the  $D_{\text{app}}$  and the  $D_{\text{appS}}$  values corresponding to the SAXS best-fitting parameters of Table 2 clearly shows the improvement in the agreement between the calculated and the experimental value that is achieved with the minimization procedure. Very similar  $D_{\text{app}}$  and  $D_{\text{appSD}}$  data are obtained at all the NaCl concentrations. No sensitive differences are pointed out between the agreements obtained with the two interaction models. As shown in Figure

7, the calculated intensity markedly disagrees with the experimental spectra at 0.1 M NaCl. However, the agreement sensitively improves at higher electrolyte concentration. As shown by the residues, the largest differences between calculated and experimental intensities are observed at low  $q$  values where the spectra are strongly affected by particle interaction, namely by the  $S(q)$  factor. The disagreement between the  $S(q)$  functions extracted by these calculated curves and those obtained by fitting only the SAXS spectra supports this result (Figure 8).

If the  $a_e/b_e$  ratios for the results reported in Tables 2 and 4 are examined we observe that the geometrical parameters obtained by minimizing the  $R_D$  factor represent more anisotropic micelles than those derived by fitting only the SAXS spectra. Large changes are also observed between the  $\alpha$  and  $t$  values of Tables 2 and 4. The higher  $\alpha$  and  $t$  values observed in Table 4 show that a stronger repulsive character of the potential tail is obtained when SAXS and DLS data are integrated in the interpretation. However, the trends of all the best-fitting parameters of Table 2 are preserved in Table 4. In particular we observe that  $a_e$  increases whereas  $b_e$  remains almost constant by increasing the NaCl concentration, thus indicating a rod-like growth of the NaTDC micelles. At the same time the decrease of the  $\alpha$ , the  $\kappa^{-1}$ , and the  $t$  values by increasing the ionic strength confirms the progressive screening of the electrostatic interaction previously described in the discussion of Tables 1–3.

It must be stressed that even the overall fitting procedure is far from giving satisfactory fits of SAXS and DLS data for the samples at low NaCl concentrations. This conclusion is testified by the bad agreement between calculated and experimental SAXS spectra shown in Figure 7 for these samples, and throws doubts on the reliability of the corresponding parameters of Table 4. The hypotheses assumed in the interpretation models must be the reason of this disagreement. These hypotheses concern both the particle structure and the interparticle interaction potential. Work is in progress to test interpretation models with more realistic interaction potentials and particle structures. However, since assumptions on two different properties are needed, no reliable conclusions have been achieved so far.

## Conclusions

A SAXS study on NaTDC micellar solutions in a range of NaCl concentrations where the electrostatic repulsion dominates the interaction potential tail was carried out. Two forms (EDL and HC interaction models) of this tail were hypothesized to interpret the experimental data. For each form three particle symmetries (spherical, oblate, and prolate) were tested. The main results that we obtained can be summarized as follows:

(1) The information on particle structure inferred by fitting the SAXS spectra is poorly affected by the choice of the function that describes the potential tail if the repulsive character of the tail is preserved.

(2) The fits of the SAXS spectra show that the sphere is unsuitable to describe the shape of the micelles. However, they do not allow the discrimination of the aggregate symmetry since satisfactory fits are obtained by assuming both the oblate and the prolate ellipsoidal geometry for the particles.

Starting from these results an analysis of SAXS and DLS data agreement was performed. In particular, for each sample, from the SAXS best-fitting parameters a  $D_{\text{app}}$  value was calculated and compared with the experimental one. The following conclusions were reached:

(1) The comparative analysis allows the determination of the micellar symmetry. As a matter of fact, the poorest agreement

between calculated and experimental  $D_{\text{app}}$  values is obtained when the oblate symmetry is hypothesized and slightly improves passing to the spherical one. On the other hand, the best agreement is realized when the prolate geometry is assumed, thus suggesting an elongated shape for the micelles, in agreement with published results.

(2) The comparison between calculated and experimental  $D_{\text{app}}$  values is sensitive to the details of the interaction potential since at the lowest NaCl concentration the best agreement of the two data is obtained when the more realistic EDL model is used.

Finally, an integrated interpretation was carried out for each sample by following a minimization procedure where the structure and the interaction parameters for the micelles were determined by searching the best fit with both the experimental SAXS and  $D_{\text{app}}$  data.

**Acknowledgment.** This work was sponsored by Italian Ministero dell'Istruzione, dell'Università e della Ricerca (Cofin no. 20020371541).

## References and Notes

- (1) Leaist, D. G.; Hao, L. *J. Phys. Chem.* **1995**, *99*, 12896.
- (2) Leaist, D. G.; Hao, L. *J. Phys. Chem.* **1993**, *97*, 7763.
- (3) Imae, T. *J. Phys. Chem.* **1988**, *92*, 5721.
- (4) Liu, H.; Skibinska, L.; Gapinski, J.; Patkowski, A.; Fischer, E. W.; Pecora, R. *J. Chem. Phys.* **1998**, *109*, 7556.
- (5) Tracy, M. A.; Pecora, R. *Macromolecules* **1992**, *25*, 337.
- (6) Corti, M.; Degiorgio, V. *J. Phys. Chem.* **1981**, *85*, 711.
- (7) Dorshow, R.; Briggs, J.; Bunton, C. A.; Nicoli, D. F. *J. Phys. Chem.* **1982**, *86*, 2388.
- (8) Dorshow, R. B.; Bunton, C. A.; Nicoli, D. F. *J. Phys. Chem.* **1983**, *87*, 1409.
- (9) Ortega, F.; Bacaloglu, R.; McKenzie, D. C.; Bunton, C. A.; Nicoli, D. F. *J. Phys. Chem. B* **1990**, *94/2*, 501.
- (10) Janich, M.; Lange, J.; Graener, H.; Neubert, R. *J. Phys. Chem. B* **1998**, *102*, 5957.
- (11) Mazer, N. A.; Carey, M. C.; Kwasnick, R. F.; Benedek, G. B. *Biochemistry* **1979**, *18*, 3064.
- (12) Schurtenberger, P.; Mazer, N.; Känzig, W. *J. Phys. Chem.* **1983**, *87*, 308.
- (13) D'Archivio, A. A.; Galantini, L.; Tettamanti, E. *J. Phys. Chem. B* **2000**, *104*, 9255.
- (14) Galantini, L.; Giglio, E.; Pavel, N. V.; Punzo, F. *Langmuir* **2003**, *19*, 1319.
- (15) D'Alagni, M.; D'Archivio, A. A.; Galantini, L.; Giglio, E. *Langmuir* **1997**, *13*, 5811.
- (16) Bonincontro, A.; Briganti, G.; D'Archivio, A. A.; Galantini, L.; Giglio, E. *J. Phys. Chem. B* **1997**, *101*, 10303.
- (17) Bonincontro, A.; D'Archivio, A. A.; Galantini, L.; Giglio, E.; Punzo, F. *J. Phys. Chem. B* **1999**, *103*, 4986.
- (18) Missel, P. J.; Mazer, N. A.; Benedek, G. B.; Young, C. Y.; Carey, M. C. *J. Phys. Chem.* **1980**, *84*, 1044.
- (19) Porte, G.; Appel, J. *J. Phys. Chem.* **1982**, *85*, 2511.
- (20) Galantini, L.; Pavel, N. V. *J. Chem. Phys.* **2003**, *118*, 2865.
- (21) Esposito, G.; Giglio, E.; Pavel, N. V.; Zanobi, A. *J. Phys. Chem.* **1987**, *91*, 356.
- (22) Galantini, L.; Giglio, E.; Leonelli, A.; Pavel, N. V. *J. Phys. Chem. B* **2004**, *108*, 3078.
- (23) Bendedouch, D.; Chen, S.-H.; Koehler, W. C. *J. Phys. Chem.* **1983**, *87*, 2621.
- (24) Bendedouch, D.; Chen, S.-H. *J. Phys. Chem.* **1984**, *88*, 648.
- (25) Bendedouch, D.; Chen, S.-H. *J. Phys. Chem.* **1983**, *87*, 1653.
- (26) Kotlarchyk, M.; Chen, S.-H. *J. Chem. Phys.* **1983**, *79*, 2461.
- (27) Long, M. A.; Kaler, E. W.; Lee, S. P.; Wignall, G. D. *J. Phys. Chem.* **1994**, *98*, 4402.
- (28) Tomšič, M.; Bešter-Rogač, M.; Jamnik, A.; Kunz, W.; Touraud, D.; Bergmann, A.; Glatter, O. *J. Phys. Chem. B* **2004**, *108*, 7021.
- (29) Hayter, J. B.; Penfold, J. *Mol. Phys.* **1981**, *42*, 109. Hansen, J. P.; Hayter, J. B. *Mol. Phys.* **1982**, *46*, 651.
- (30) Percus, J. K.; Yevick, G. J. *Phys. Rev.* **1958**, *110*, 1.
- (31) Siegert, A. J. F. *MIT Rad. Lab. Rep. No.* **1943**, 465.
- (32) Koppel, D. E. *J. Chem. Phys.* **1972**, *57*, 4814.
- (33) Pusey, P. N.; Tough, R. J. A. In *Dynamic Light Scattering*; Pecora, R., Ed.; Plenum: New York, 1985; Chapter 4.
- (34) Dhont, J. K. G. *An Introduction to Dynamics of Colloids*; Möbius, D., Miller, R., Eds.; Elsevier: Amsterdam, The Netherlands, 1996.
- (35) Felderhof, B. U. *J. Phys. A* **1978**, *11*, 929.
- (36) Ornstein, L. S.; Zernicke, F. *Proc. Akad. Sci.* **1914**, *17*, 793.
- (37) Durchschlag, H.; Zipper, P. *J. Com. Esp. Deterg.* **1995**, *26*, 275.
- (38) Matsuoka, K.; Maeda, M.; Moroi, Y. *Colloids Surfaces B* **2003**, *32*, 87.
- (39) Stabinger, H.; Kratky, O. *Makromol. Chem.* **1978**, *179*, 1655.
- (40) Glatter O. *J. Appl. Crystallogr.* **1974**, *7*, 147.
- (41) Verwey, E. J. W.; Overbeek, J. Th. G. *Theory of the Stability of Lyophobic Colloids*; Elsevier: New York, 1948.
- (42) Galantini, L.; Giampaolo, S. M.; Mannina, L.; Pavel, N. V.; Viel, S. *J. Phys. Chem. B* **2004**, *108*, 4799.
- (43) Cichocki, B.; Felderhof, B. U. *J. Chem. Phys.* **1991**, *94*, 556.
- (44) Thiele, E. *J. Chem. Phys.* **1968**, *39*, 474.
- (45) Wertheim, M. S. *Phys. Rev. Lett.* **1963**, *10*, 321.
- (46) Tanford, C. *Physical Chemistry of Macromolecules*; Wiley: New York, 1961.
- (47) Perrin, F. *J. Phys. Radium* **1936**, *7*, 1.
- (48) Herzog, R. O.; Illig, R.; Kudar, H. Z. *Phys. Chem.* **1934**, *A 167*, 329.
- (49) Belloni, L.; Drifford, M. *J. Phys. Lett.* **1985**, *46*, L-207.
- (50) Belloni, L.; Drifford, M. *J. Phys. Lett.* **1985**, *46*, L-1183.